




Seismic response of granites with different grain sizes after thermal treatment: an experimental study

Erkang Zhou · Tianqi Zhai · Jianbo Zhu 

Received: 4 March 2023 / Accepted: 1 October 2023
© The Author(s) 2023

Abstract Understanding the wave propagation behaviour in rock masses with different temperatures and geological conditions is of great significance for the stability and safety evaluation of deep rock engineering, e.g., enhanced geothermal system, nuclear waste disposal. However, the response and mechanism of ultrasonic waves through granites after thermal treatment are still poorly understood. In order to determine the combined effects of heating temperature and grain size on wave propagation across granites, a series of laboratory ultrasonic tests were performed with the pulse transmission method, combined with scanning electron microscopy observation. The testing results indicate that heating temperature and grain size have a combined impact on wave propagation across the tested granites. The wave velocity, transmitted coefficient, peak power spectral density

and accumulative energy are generally negatively correlated with heating temperature regardless of grain size. The effect of grain size on wave propagation is more pronounced at low temperatures. Basically, the crack evolution is the main reason for the seismic response of granite after thermal treatment. A damage factor defined by the change of microcrack area in this paper is proposed and adopted to consider the combined effect of heating temperature and grain size. The peak power spectral density of the low-frequency wave and the transmission coefficient of the high-frequency wave are appropriate as the optimal wave indicators for evaluating the deterioration of granites at high- and low-damage stages, respectively. The findings in this study are of great importance for site selection and stability assessment in rock engineering activities under high temperatures, especially for the development of deep-seated hot dry rock.

E. Zhou · T. Zhai
State Key Laboratory of Hydraulic Engineering
Simulation and Safety, School of Civil Engineering,
Tianjin University, Tianjin, China

T. Zhai
China Railway Siyuan Survey and Design Group Co.,Ltd,
Wuhan, China

J. Zhu (✉)
Guangdong Provincial Key Laboratory of Deep
Earth Sciences and Geothermal Energy Exploitation
and Utilization, Institute of Deep Earth Sciences
and Green Energy, Shenzhen University, Shenzhen, China
e-mail: jianbo.zhu@szu.edu.cn

Article Highlights

- The multi-frequency seismic responses of granites with different grain sizes after thermal treatment are comprehensively studied.
- The mechanism of microcrack evolution under the combined effects of heating temperature and grain size are experimentally analysed.
- The wave indicators for evaluating the deterioration of granites are proposed by considering the

relationship between wave attenuation and damage.

Keywords Thermal treatment · Grain size · Wave propagation · Microcrack evolution · Damage

1 Introduction

Multiple deep rock engineering activities are carried out in high-temperature conditions and complex geological environments, e.g., geothermal energy development (Hu et al. 2019) and nuclear waste disposal (Dwivedi et al. 2008). Thermal fractures generally develop in rocks under high temperatures, which is the main reason for rock deterioration (Yang et al. 2017). Rock microstructure, e.g., grain size, considerably influences the fracture behaviour of rocks (Shao et al. 2015). Elucidating the fracture behaviour of rocks is essential to rationally utilize thermal resources and effectively prevent thermal disasters. Additionally, seismic wave parameters such as wave velocity and amplitude could be used for fracture detection and stability assessment of rock masses (Chen et al. 2017; Zhu et al. 2020). Although the effects of temperature and grain size on rock properties and fracture behaviour have been extensively investigated (Zhao et al. 2018; Feng et al. 2021; Zhai et al. 2022), the response and mechanism of ultrasonic waves through granites under the combined effects of heating temperature and grain size are still poorly understood. Therefore, it is of great significance to investigate the ultrasonic wave propagation through granites with different grain sizes after thermal treatment.

Many features of ultrasonic wave propagation have been proven to be affected by the heating temperature of rocks, e.g., wave velocity (Griffiths et al. 2018), waveform (Inserra et al. 2013), spectral amplitude (Chaki et al. 2008) and power spectral density (PSD) (Dehghani et al. 2020). Among these topics, the evolution of ultrasonic wave velocity induced by thermal stress is the earliest and most widely studied. Menendez et al. (1999) used ultrasonic pulse transmission techniques to measure P-wave velocities along three orthogonal directions and found that the anisotropies of acoustic velocities in thermally damaged and intact granites are comparable. Fan et al. (2017) performed a

series of ultrasonic tests to investigate thermal effects on the wave velocity and P-wave modulus, finding that they decline monotonously with increasing temperature. Zhang et al. (2021a, b) stated that P- and S-wave velocities at six various frequencies decrease with increasing temperatures from 25 to 500 °C, and the reduction amplitude of the P-wave is larger than that of the S-wave. Inserra et al. (2013) studied the change in transmitted waveforms for granites under different temperatures and concluded that there are no dramatic variations when the temperature is lower than 500 °C. Spectrum analysis of ultrasonic waves, derived from the Fourier transformation, is another important way to study wave propagation (Cerrillo et al. 2014). Chaki et al. (2008) conducted ultrasonic testing of granites at temperatures from 100 to 600 °C and reported that there is a regular decrease in the central spectral amplitude and complete dissipation of ultrasonic energy below 500 °C. Dehghani et al. (2020) reported that thermal treatment has no significant influence on frequency components but plays a role in reducing the peak value of the PSD. Additionally, a signal processing approach (i.e., wavelet analysis and filtering) is utilized to analyse the distribution characteristics of ultrasonic energy with high resolution (Zhang et al. 2019). Sun et al. (2022) employed the wavelet packet decomposition method to evaluate the energy proportions in each sub-band for ultrasonic waves across granites at high temperatures from 200 to 600 °C and found that the fractured cores reduce the proportion of high-frequency energy with increasing temperature.

It is worth noting that the attributes of mineral particles, especially grain size, should be considered as crucial parameters that directly affect the wave propagation behaviour across granites. Vajdova et al. (1999) found a negative correlation between the average grain size (from 0.03 to 0.11 mm) and mean P-wave velocity, which can be explained by the scale problem of signal frequency and the elastic properties of materials. Sajid et al. (2016) performed several ultrasonic wave experiments to determine the P-wave velocities of granites with different grain sizes and found that there is a nonlinear correlation between wave velocity and grain size. Furthermore, the mechanism of the effect of grain size on the acoustic properties of rocks has received much attention. Micro-cracks generally originate at the mineral particle boundary tip, and the generation and extension of cracks induced

by differences in grain size vary considerably, thereby influencing the physical properties of rock samples (Tian et al. 2020). Machek et al. (2007) quantitatively and qualitatively investigated the influence of grain microstructure and boundary on the magnitude and anisotropy of wave velocity based on the SEM-EBSD method and reported that the grain size of the rock forming minerals controls the amount of microporosity. Li et al. (2020) found that the shape and size of individual mineral grains play a key role in determining the microcrack characteristics (i.e., length and orientation) through the fluorescent dye impregnation technique.

Considering the fact that both temperature and grain size have a significant effect on wave propagation, some scholars have studied the combined effects of the two on rock deterioration in recent years. Among the limited efforts, Tian et al. (2020) and Yin et al. (2021) conducted numerical and experimental studies on the mechanical characteristics of granites with different grain sizes after heat treatment, finding that the mechanical properties of the coarse-grained granite are more deteriorated than those of the fine-grained granite. Ersoy et al. (2021) reported that fine crystals are more resilient to thermal stress since they expand hinged during heating, whereas coarse crystalline rocks undergo severe thermal damage. However, the response and mechanism of ultrasonic waves to the combined effects of temperature and grain size have not been investigated yet. And the evaluation metrics and characterization methods based on ultrasonic wave propagation for this combined effect have still not been proposed.

In this study, ultrasonic wave transmission experiments are performed to investigate the combined effects of heating temperature and grain size on ultrasonic wave propagation across granites. Based on the Fourier transformation and wavelet packet

decomposition methods, the characteristic ultrasonic wave features, i.e., wave velocity, transmission coefficient, peak PSD and accumulative energy, are utilized to describe the wave propagation behaviour. Scanning electron microscope (SEM) and image threshold technology are applied to investigate the development of thermally induced micro-cracks and to quantitatively characterize the damage degree at the microscopic scale. According to the sensitivity of propagation features, the evaluation indicators of ultrasonic waves with different central frequencies are proposed for evaluating the deterioration of granites. The findings in this study are of great significance for site selection and stability assessment in geothermal engineering in granite masses.

2 Experimental equipment and method

2.1 Sample preparation

Granite is a heterogeneous entity composed of diverse mineral grains, which is usually classified as coarse- (> 5 mm), medium- (1–5 mm) and fine-grained (< 1 mm) granite based on the average grain size of the constituent mineral grains (Qiu 1991). In this study, granites from three origins were carefully selected to represent rocks of different grain sizes. According to the average grain size, the rock samples were classified into three types: fine-grained granite (FG), medium-grained granite (MG) and coarse-grained granite (CG). Their corresponding origins are Laizhou, Shandong Province, Suizhou, Hubei Province and Rizhao, Shandong Province, respectively. Table 1 shows the average grain sizes and mineral compositions of FG, MG and CG. Notably, the mineral compositions of the three sample types selected are highly similar, which mitigates the potential

Table 1 Grain sizes and contents of constituted minerals in FG, MG and CG specimen

Sample	Average grain size/mm	Mineral composition
FG	1.2	Potassium feldspar phenocryst (12.5 mm, 17%); Potassium feldspar (3.5 mm, 20%); Plagioclase (3.5 mm, 40%); Quartz (3.5 mm, 20%); Mica (0.5 mm, 3%)
MG	3.4	Potassium feldspar (3.5 mm, 37%); Plagioclase (3.5 mm, 40%); Quartz (3.5 mm, 20%); Mica (0.5 mm, 3%)
CG	5.0	Potassium feldspar (1.2 mm, 33%); Plagioclase (1.3 mm, 45%); Quartz (1.3 mm, 20%); Mica (0.5 mm, 2%)

Note that the average grain size of granite is estimated based on the particle size and content of the constituted minerals

impact of different mineral compositions on thermal fracture behaviour. All samples were manufactured into short cylinders of $\Phi 50 \text{ mm} \times 50 \text{ mm}$ by coring and turning to meet ASTM standards (D2845-08 2008) for ultrasonic testing. Three parallel testing sessions were conducted on rock samples of each group to mitigate the influence of grain size discrepancies on the experimental results.

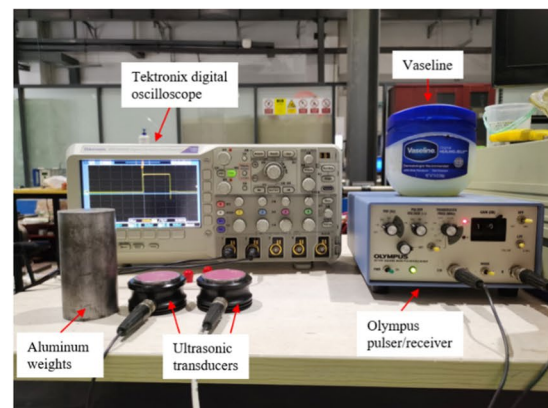
2.2 Experimental apparatuses and procedures

In this study, a programmable high-temperature heating furnace (as shown in Fig. 1a) facilitated the heating process of thermal treatment. The temperatures of the granite samples were set to increase from room temperature to the target temperature of 200, 400, 600, or 750 °C at a constant heating rate (i.e., 9 °C/min) and to be constant for a sufficiently long period (i.e., 3 h). After that, the granite specimens were cooled in the air to room temperature. The determination of the heating rate and constant temperature time refers to previous work (Ersoy et al. 2021) to minimize thermal shock and obtain sufficient thermal fracture.

Ultrasonic measurements were performed on granites after heating by using the ultrasonic test system (see Fig. 1b), which consists of an Olympus pulser/receiver (model 5077PR), a Tektronix digital oscilloscope (model DPO 2012B), and a pair of ultrasonic transducers (i.e., a transmitter and a receiver). A high-voltage pulse is provided by the Olympus pulse generator to the selected transducer at the corresponding central frequency, generating ultrasonic waves outward. The ultrasonic signal through the rock sample is received by the transducer and converted into an electrical signal, which is then transmitted to the Olympus pulse receiver. Attached to the Olympus pulser/receiver, the Tektronix digital oscilloscope is used to digitize, present and record a section of the entire transmitted signal at a constant sampling frequency (i.e., 125 MHz). In addition, two types of incident waves with a central frequency of 0.1 MHz (LF wave) and 1.0 MHz (HF wave) were applied in the ultrasonic tests on the same specimens, considering the equipment available in our laboratory and referring to previous research findings (Yang et al. 2019, 2020). The introduction of LF and HF waves helps to clarify the effects of incident wave bandwidth on



(a)



(b)



(c)

Fig. 1 The experiment apparatuses: **a** Muffle furnace; **b** ultrasonic test system; **c** scanning electron microscopy (SEM) machine

wave propagation of thermally damaged granites with different grain sizes. Note that the ultrasonic tests were repeated three times to ensure the accuracy of the experimental data.

The micro-structural variations of minerals in rock samples were identified by performing SEM analysis to understand the effect of heating temperature and grain size on crack evolution. A desktop SEM machine (model Phenom XL) in a low-vacuum environment was used to capture the microscopic fracture morphology of the granite, combined with an electron backscattered diffraction (EBSD) scanning technique, as shown in Fig. 1c. The EBSD technique was used for high-speed phase mapping and crystallographic studies of the granite specimens. The SEM analysis was conducted on fresh sections of granites before and after heating in this study. It should be emphasized that the scanning area before and after heating is the same to track the evolution of micro-cracks. Before the SEM analysis, a manual holder was applied to stabilize the granite to obtain clear images while suppressing the charging effect on the sample surface. Furthermore, the SEM observation magnification was chosen to be 265 times with a view range of 1.01×1.01 mm.

2.3 Analysis methods

The full wave train of an ultrasonic signal is composed of the primary wave and the later arrival (Sang et al. 2020). The primary pulse signal carries a large amount of information in response to the rock structure, which has an important role in characterizing the ultrasonic wave propagation behaviour through granites (Benavente et al. 2020). In this study, the primary wave was captured to exclude the multiple fusion influence of reflected and refracted waves caused by inhomogeneous media and structural interfaces within the rock sample.

2.3.1 Wave velocity

According to the ultrasonic pulse transmission technique recommended by ASTM Standard (D2845-08 2008), the ultrasonic longitudinal wave velocity of granite after high-temperature treatment can be calculated by

$$V_p = \frac{L}{t - t_0} \quad (1)$$

where L is the total length of the rock specimen, which is measured by a Vernier calliper with an accuracy of 0.01 mm, t is the travel time of the signal through the rock specimen determined by the take-off point, where the signal voltage first declined dramatically, and t_0 is determined by the system delay time between the transmitting and receiving sensors. The take-off point of the ultrasonic wave (see Fig. 2a), is determined by a self-programmed code to ensure the accuracy of the travel time.

2.3.2 Wave transmission

The transmission behaviour of ultrasonic waves could be influenced by the development of micro-defects in rock samples. When evaluating the wave transmission property, the ultrasonic wave through granites at room temperature is regarded as the reference pulse. Wave transmission capacity is generally described by the transmission coefficient, which is defined as the ratio between the amplitude of the transmitted wave and the reference wave (Yang et al. 2019). The wave amplitude is the voltage difference between the wave crest and trough of the primary pulses, as shown in Fig. 2a. Thus, the transmission coefficient T could be calculated by the wave amplitude through granites before and after heating:

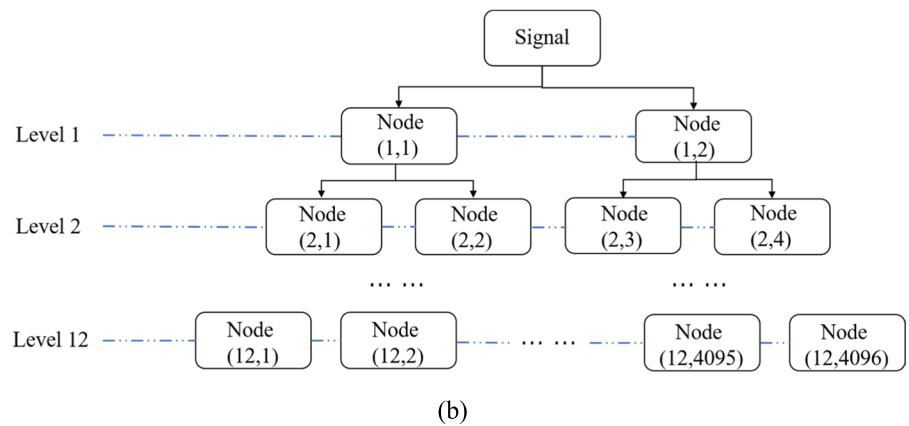
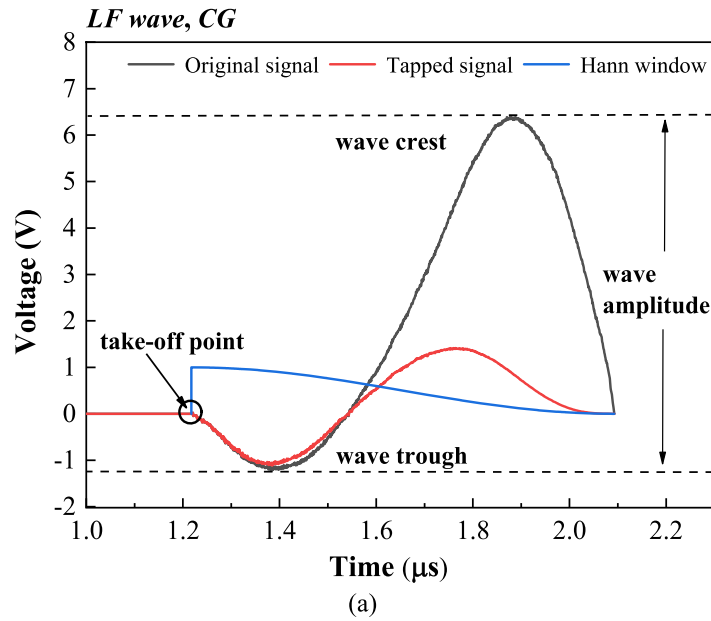
$$T = \frac{A_h}{A_r} \quad (2)$$

where A_h and A_r are the wave amplitudes of the primary ultrasonic wave through high-temperature and room-temperature treated granites, respectively.

2.3.3 Spectral analysis

Rock material is a natural low-pass filter for ultrasonic waves, with the role of frequency-selective absorption (Yang et al. 2020). Spectrum analysis can provide information on the frequency characteristics of ultrasonic waves through granites. The PSD of an ultrasonic signal is defined as the signal spectral power over a unit frequency band. The results of Dehghani et al (2020) have shown that PSD is more closely related to the damage degree and microcrack

Fig. 2 Examples of data processing: **a** Tapering process of original ultrasonic signal and determination of take-off point; and **b** 12-layer wavelet packet decomposition schematic diagram



evolution induced by thermal loading compared to the frequency amplitude. The PSD is generally estimated by the periodogram method (Zhou and Xie 2004). The waveform signal $f(n)$ in the form of discrete points obtained by sampling can be transformed into the frequency spectrum signal $F(\omega)$ using the discrete Fourier transform (Wang et al. 2019). The power spectrum signal $P(\omega)$ can be calculated as

$$F(\omega) = \sum_{n=0}^{N-1} f(n)e^{-j2\pi n\omega/N}, \quad 0 \leq \omega \leq N - 1$$

$$P(\omega) = \lim_{N \rightarrow \infty} \frac{|F(\omega)|^2}{N} \tag{3}$$

where N is the number of discrete points. Additionally, based on the study of Yang et al. (2019), the original signal was processed by adding a Hann window (as shown in Fig. 2a) to highlight the low-frequency information and filter the irrelevant high-frequency information of original signals.

2.3.4 Wave energy

The dispersion and dissipation extent of wave energy in a specific frequency band is highly dependent on the evolution of fractures with characteristic scale (Fjær et al. 2013; Ding et al. 2020). Therefore, recording the distribution of signal energy over sub-bands is helpful to understand the

change in the crack scale. To ensure the high resolution of the sub-band and avoid energy loss, wavelet packet decomposition is introduced to achieve multiple decompositions of ultrasonic signals (Galiana-Merino et al. 2013). The energy of the reconstructed signal for each frequency band $E_{j,k}$ can be expressed as

$$E_{j,k} = \int |s_{j,k}(t)|^2 dt = \sum_{l=1}^m |y_{k,l}|^2 \tag{4}$$

where $s_{j,k}$ is the reconstructed signal of the k th band in the j th layer, with $k=0, 1, 2, \dots, 2^j - 1$, and $y_{k,l}$ represents the amplitude of the discrete sampling with the number m . The accumulative energy E_0 of the signal and the energy ratio per sub-band η are calculated by Eq. (5) and (6), respectively:

$$E_0 = \sum_{k=0}^{2^j-1} E_{j,k} \tag{5}$$

$$\eta = \frac{E_{j,k}}{E_0} \times 100\% \tag{6}$$

The ‘db7’ wavelet was chosen in this study because of the lower reconstruction error and a better division of frequency bands (Liang et al. 2020). In our ultrasonic tests, the sampling frequency is

125 MHz, and the corresponding Nyquist frequency is 62.5 MHz. As indicated by Sun et al. (2022), the signal bandwidth should be several times the sub-band bandwidth to effectively display the energy distribution of ultrasonic wave signals in the frequency spectrum. Thus, after many attempts, the layers of wavelet decomposition were chosen as 12 and 11 for the ultrasonic wave with incident frequencies of 0.1 and 1.0 MHz, respectively. Figure 2b shows the wavelet decomposition result of the ultrasonic wave with an incident frequency of 0.1 MHz. It can be seen that the 12-layer decomposition could generate 4096 (2^{12}) sub-bands, and the bandwidth of each frequency band is 15,258.8 Hz. The wavelet decomposition result of the ultrasonic wave with the incident frequency of 1.0 MHz is similar to that shown in Fig. 2b, the number of sub-bands produced is 2048 (2^{11}), and the bandwidth of each frequency band is 30,517.6 Hz.

3 Testing results

3.1 Thermal effects on wave propagation

3.1.1 Wave velocity

Figure 3a, b present the LF and HF wave velocities of granites with various thermal treatments

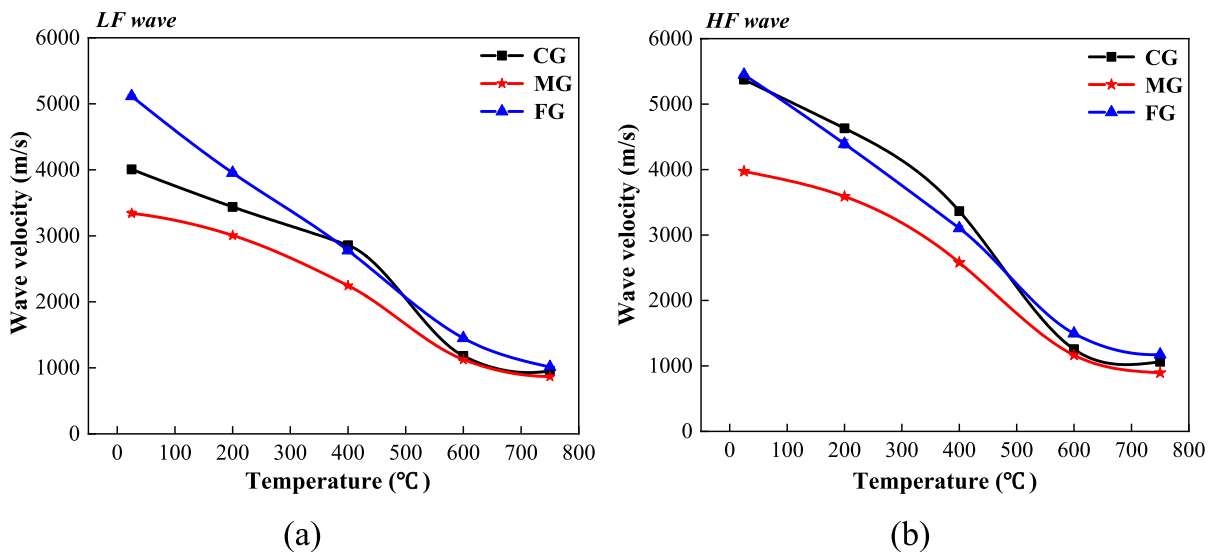


Fig. 3 Variation in wave velocity of ultrasonic wave through granites with different grain sizes and heat treatment temperatures: **a** LF wave; and **b** HF wave

and grain sizes, respectively. For the LF wave, it could be concluded that the wave velocities of FG, MG and CG granites continued to decrease with increasing temperature. The wave velocity of CG and MG granites dropped slowly with the increase in temperature from 25 to 200 °C, while that of FG granite decreased sharply. When the temperature increased from 200 to 400 °C, the wave velocity of the granite declined moderately. The greatest reduction in wave velocity occurred in the temperature range of 400–600 °C. This phenomenon could be elucidated by the progressive development of microcracks within the rock and the diminishing connection among the constituent particles. As the elastic wave passed through the heated rock, the internal traveling wave resistance increased, resulting in a significant decrease in the wave velocity (Sun et al. 2022). However, the downward trend of the wave velocity became subtle when the temperature exceeded 600 °C. For the HF wave, there was a similar tendency for the wave velocity to decrease gradually with increasing temperature, while the largest decrease was also observed between 400 and 600 °C. For instance, after heat treatment at 200, 400 and 600 °C, the wave velocity of the CG granite declined by 13.8%, 37.4% and 76.6%, respectively. Compared to the LF wave, the

HF ultrasonic wave was more severely attenuated and had a more dramatic reduction in wave velocity across thermally damaged rocks, which is in good agreement with the literature (Zhang et al. 2021a, b).

3.1.2 Transmission coefficient

Figure 4 shows the transmission coefficients of ultrasonic waves with different central frequencies across CG, MG and FG granites versus thermal treatment temperature. For the LF wave, the transmission coefficient generally tended to rise from 25 to 200 °C and then fell with increasing temperature. For instance, when the thermal treatment temperature was 200 °C, the transmission coefficient of the LF wave through MG granite increased slightly by 7.1% compared to that at room temperature. A similar trend of a moderate rise in the mechanical properties of rocks up to 200 °C has also been reported (Jiang et al. 2018; Kumari et al. 2019). This could be understood as the improvement of rock properties caused by the progressive closure of primary cracks inside the specimen due to the crystal expansion. In contrast, there is a different pattern of variation in the HF wave. The transmission coefficients of HF waves through

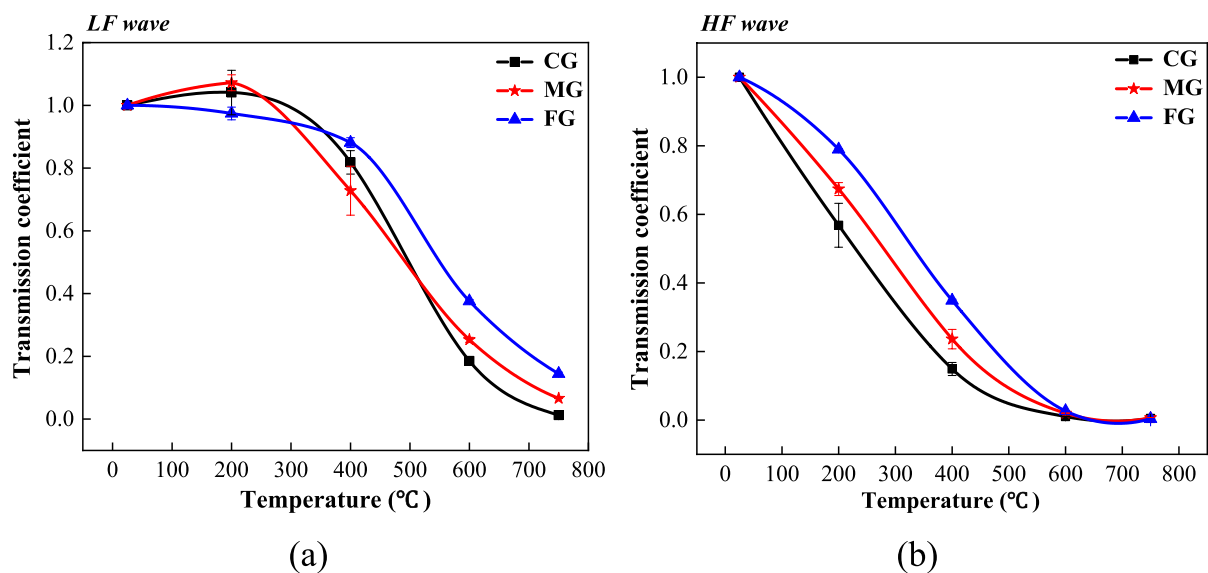


Fig. 4 Transmission coefficients of ultrasonic wave across granites with different grain sizes and heating temperatures: **a** LF wave; and **b** HF wave

granites tended to decrease with increasing temperature from 25 to 600 °C and changed slowly over 600 °C. It is widely recognized that the dramatic decline in the transmission coefficient can be primarily attributed to the heightened levels of transmission and reflection behaviour that take place across multiple interfaces within the medium. Moreover, thermal effects on the transmission coefficient are highly related to the frequency of ultrasonic waves, which is

related to frequency dispersion and scattering effects, as discussed in detail below.

3.1.3 Power spectral density

Based on the fast Fourier transform (Cerrillo et al. 2014) and Eq. (3), the PSD is calculated and derived from the original waveform. The form of variation in the power spectrum is similar when ultrasonic waves through granites with different grain sizes.

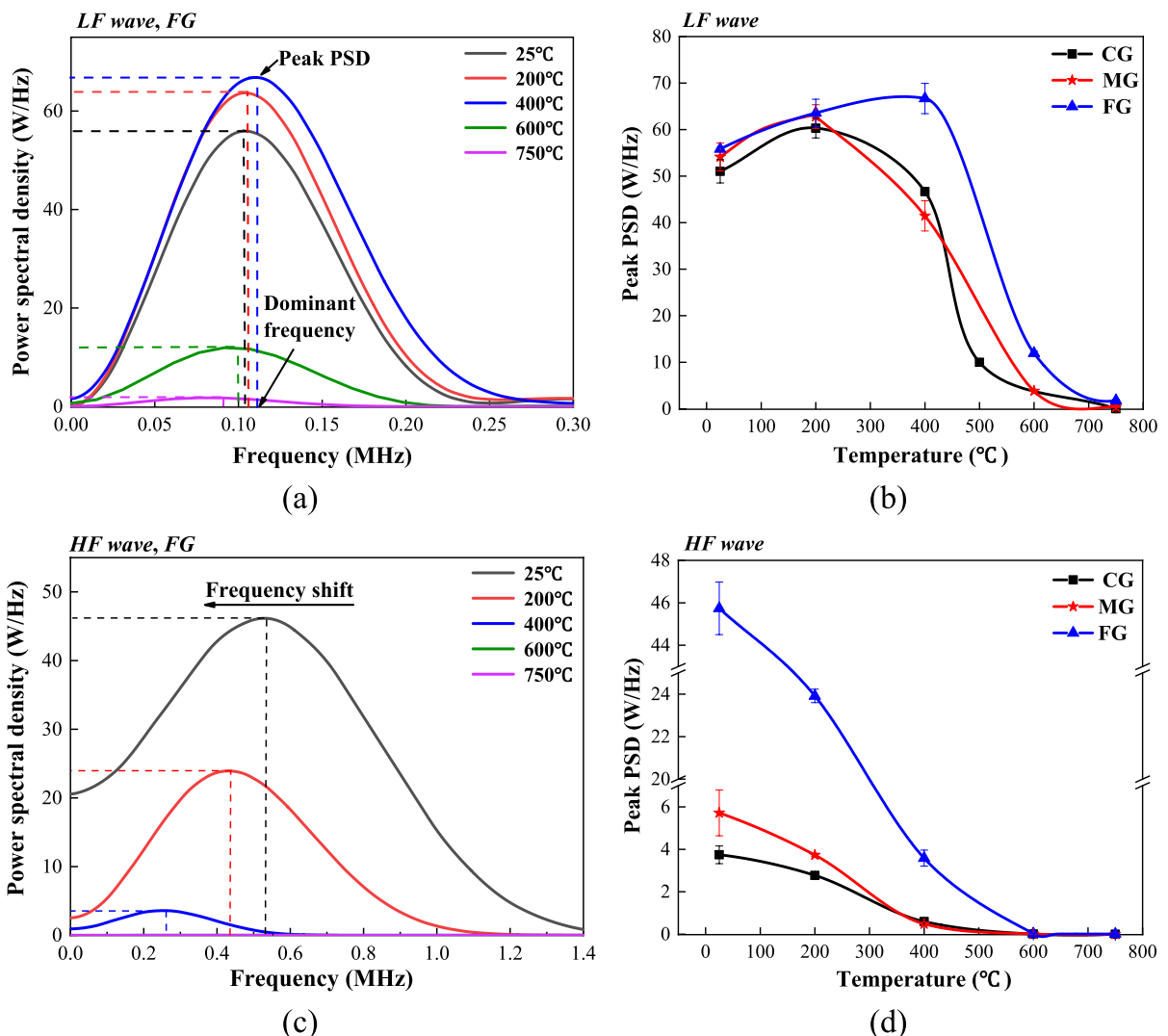


Fig. 5 Power spectrum properties of ultrasonic waves through rock samples under high temperatures: **a** and **c** For the power spectral density of LF and HF waves through FG granites versus frequency, respectively; **b** and **d** for the peak PSD of LF and HF waves across granites with different grain size,

respectively. Note that the power spectral density of the HF wave across FG granites at temperatures of 600 and 750 °C is extremely small, which is not easy to indicate in the figure, but does not affect the overall trend

Therefore, we performed a case study of the FG granite. The PSD versus frequency curves of LF and HF waves across FG granite after five temperature treatments with different gradients are shown in Fig. 5a, c, respectively. The PSD of the wave signal was concentrated in the low-frequency region and tended to zero in the high-frequency region. The PSD magnitude of the LF wave increased moderately as the temperature rose up to 400 °C. Above 400 °C, the PSD magnitude decreased substantially. However, the dominant frequency of LF waves always fluctuated within a narrow range of approximately 0.1 MHz. For the HF wave, there was a continuous reduction in the PSD magnitude with increasing temperature. The PSD of the HF wave manifested so small beyond 600 °C that it was difficult to observe. The dominant frequency of HF waves through granites after heating decreased significantly with increasing temperature. An apparent occurrence of spectral drift could be observed, which is consistent with results reported in previous studies (Chaki et al. 2008). Note that an obvious high-frequency filtering phenomenon could be seen at room temperature. This was confirmed by the fact that the dominant frequency of the LF wave is around 0.1 MHz, which is close to its central frequency, whereas that of the HF wave is 0.55 MHz, far less than its central frequency. It may be accounted for rock features as low-pass filters, which are more severe for HF waves (Yang et al. 2020).

Figure 5b, d demonstrate the peak PSD, which is the maximum value of the entire power spectral density profile, of LF and HF ultrasonic waves through granites with different thermal treatments and grain sizes, respectively. For the LF wave, the results showed that the peak PSD increases slightly initially and then decreases rapidly with increasing temperature, which is similar to the variation of transmission coefficient. The temperature of the trend transition is related to grain size. Concretely speaking, the peak PSD of the LF wave across FG granite rose steadily with increasing temperature until 400 °C (increased by about 20%), while that across CG and MG granites increased only to 200 °C (an increase of approximately 17%). In contrast, a steady decline in the peak PSD of HF waves could be found with increasing temperature. When the temperature increased from room temperature to 600 °C, the peak PSD of FG granite decreased from 45.7 to 0.02 W/Hz, and its attenuation amplitude was significantly higher than

that through CG and MG granites. When the heating temperature was higher than 600 °C, the measured peak PSD was too small to analyse.

3.1.4 Energy distribution and accumulation

Based on the wavelet packet decomposition method, the wave energy distribution and accumulation are obtained by Eqs. (6) and (5), respectively. Figure 6a, c present the energy distribution curves of LF (first sixteen sub-bands) and HF waves (first forty-two sub-bands) across FG granites after heating treatment, respectively. Owing to the low-pass filtering characteristics of rocks, the energy ratio of high-frequency sub-bands is extremely low and the wave energy is focused on a few low-frequency sub-bands. Thus, to analyse the energy distribution efficiently, only the sub-bands with an energy ratio higher than 0.1 (effective sub-bands) were presented. The energy distribution could be analysed from two aspects: the dominant frequency band (maximum energy ratio position) and the bandwidth (range of effective frequency bands). For the LF wave, as the temperature increased, the dominant frequency band slowly transferred to the lower frequency region accompanied by an increase in the maximum energy ratio. However, the bandwidth of the LF wave had no change as the temperature increased from 25 to 600 °C (all are 14 sub-bands), and decreased to 9 sub-bands at 750 °C. This could be explained that the LF wave has a long wavelength and responds significantly to large-size cracks, which develop slowly and limitedly under low-temperature conditions.

For the HF wave, the decentralized energy distribution apparently became concentrated with increasing temperature. The bandwidth of the HF wave at room temperature was considerably larger with forty-two sub-bands while the maximum energy ratio of that was relatively less (15%), meaning a decentralized energy distribution of the HF wave at the initial state. As the temperature rose to 750 °C, the bandwidth dropped steeply to seven sub-bands, with a maximum energy ratio of 42%, reflecting an obvious energy concentration behaviour. It also could be seen that as the temperature rose from 25 to 750 °C, the dominant frequency band of the HF wave shifted from high (22nd sub-bands) to low frequencies (2nd sub-bands). The obvious concentration trend of the HF wave energy with increasing temperature could be

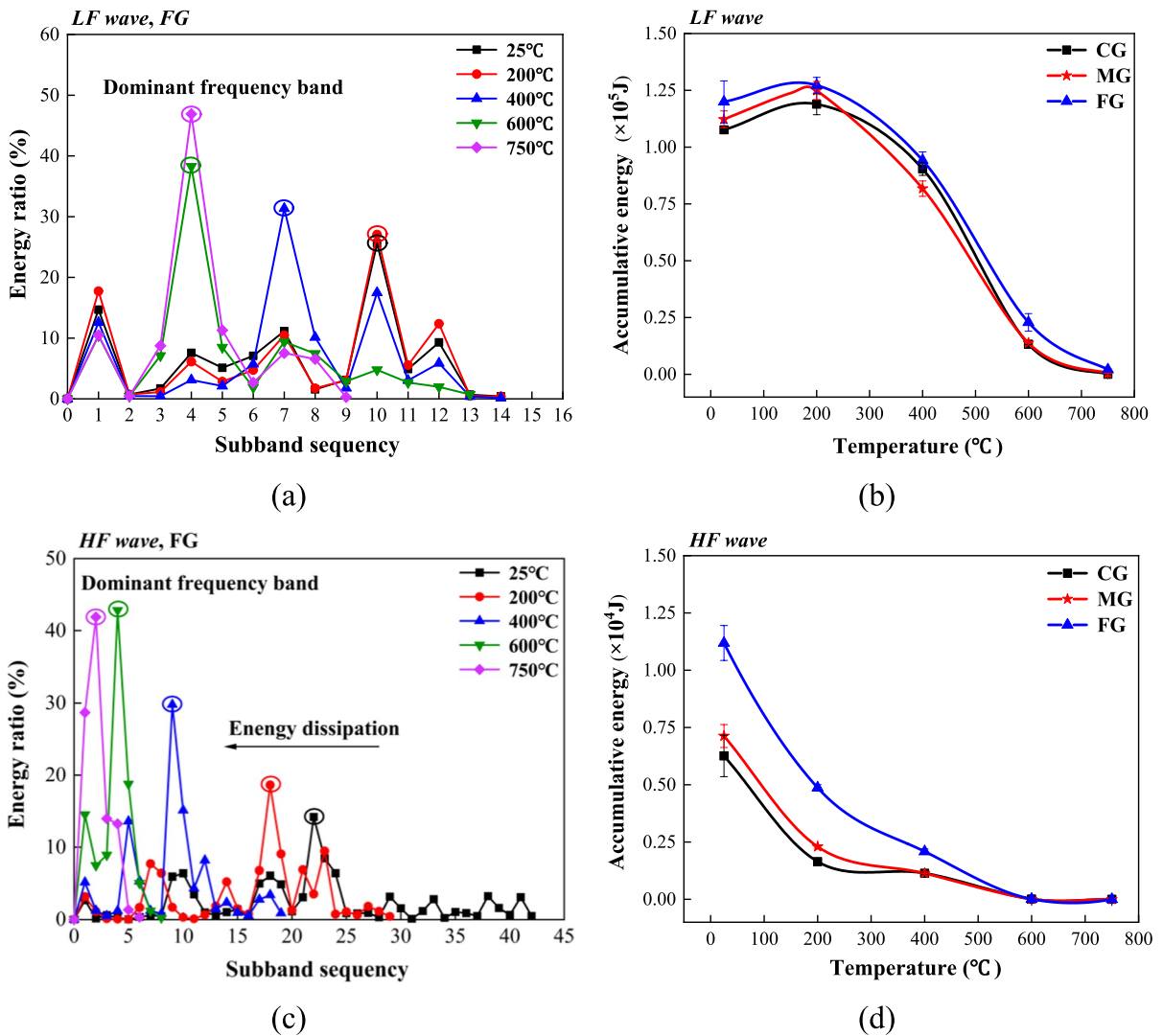


Fig. 6 Energy distribution and accumulation of waves through rock specimen after heat treatment: **a** and **b** For the energy distribution in each frequency band and the accumulative energy

of LF waves across granites, respectively; **c** and **d** for the energy distribution and accumulative energy of HF ultrasonic waves, respectively

explained that cracks in the specimens gradually initiate and develop to a larger scale, resulting in a shift of wave energy to lower frequencies.

There is a significant difference in the energy distribution between HF and LF waves, which may be attributed to the different evolution of the characteristic scale fracture. For instance, when the temperature increased from 25 to 200 $^{\circ}$ C, the energy distribution of the LF wave changed less, while the energy of the HF wave concentrated to lower frequencies, indicating an abundance of small-size cracks sensitive to HF

waves developing progressively. In addition, at the temperature from 600 to 750 $^{\circ}$ C, the bandwidth of the LF wave decreased from 14 to 9 sub-bands with an increased maximum energy ratio (about 10%). However, the dominant frequency band of the HF wave shifted from the 4th to the 2nd sub-band with the constant bandwidth and a slight decrease in the maximum energy ratio, corresponding to the transition of cracks expanding from microscopic to macroscopic scales.

Figure 6b, d illustrate the variation in accumulative energy of LF and HF ultrasonic waves through granites with various grain sizes after five different thermal treatment levels, respectively. It could be seen that the change regularity of the accumulative energy is similar to the transmission coefficient and the peak PSD. Generally speaking, there was a moderate increase in the accumulative energy of the LF wave when the thermal treatment temperature was below 200 °C. Beyond 200 °C, the accumulative energy declined sharply with increasing temperature, in which the maximum decrease occurred in the temperature interval of 400–600 °C. For the HF wave, the accumulative energy declined moderately with increasing temperature. When the temperature increased from 25 to 600 °C, the accumulative energy of the HF wave dropped markedly by approximately 99%, while the decreasing trend became quite subtle beyond 600 °C. By comparison, it could be drawn that the central frequency plays a significant role in wave energy behaviours. For instance, when the temperature was less than 200 °C, the accumulative energy of the LF wave increased slightly, while under the same condition, that of the HF wave declined. This could be explained by the fact that primary defects close due to the crystal expansion, which highly affects the LF wave rather than the HF wave.

3.2 Effects of grain size on wave propagation

3.2.1 Wave velocity

Figure 7a, b exhibit the variations in LF and HF wave velocities through granites with different grain sizes after thermal treatment, respectively. Regardless of the central frequency of ultrasonic waves, the wave velocities of granites showed a V-shaped trend with increasing grain size, which is consistent with results reported in previous research (Sajid et al. 2016). Moreover, the variations in wave velocities among the three kinds of samples declined with increasing temperature. For instance, the LF wave velocities of CG, MG and FG granites were 4007, 3341 and 5115 m/s at room temperature of 25 °C, respectively. At a heating temperature of 750 °C, the LF wave velocities of CG, MG and FG granites were 955, 868 and 1011 m/s, respectively. It means that the wave velocities of granites are highly dependent on the grain size, especially at lower temperatures. The vast differences in velocities under low-temperature conditions may be caused by the presence of primary fractures related to grain size. As the temperature increased and thermal cracks developed, the fracture differences gradually eliminated, and wave velocities of rocks with different grain sizes tended to be the same.

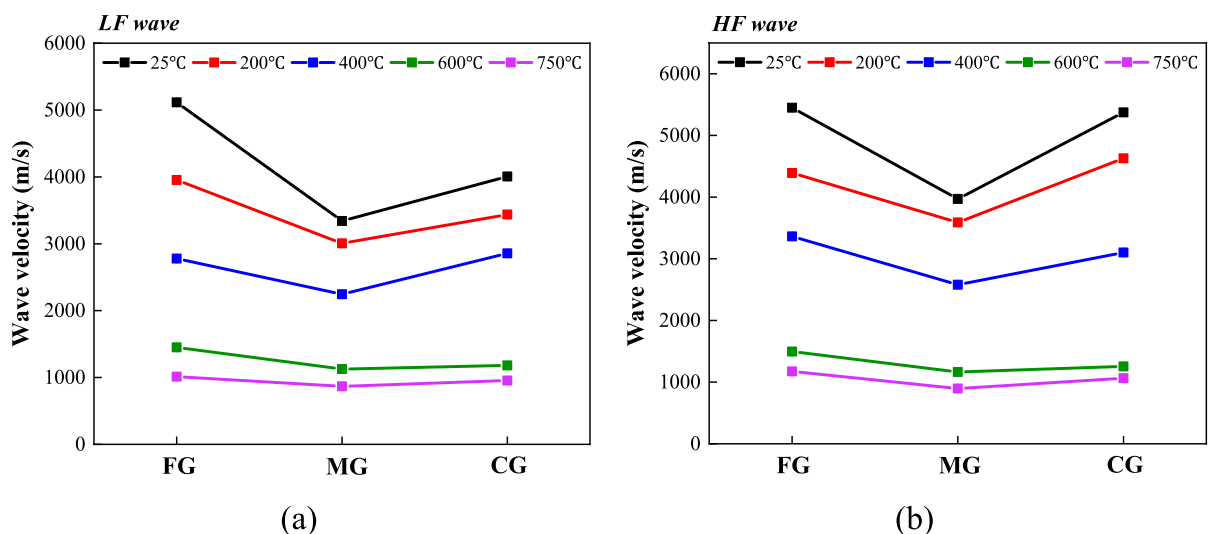


Fig. 7 Variation in wave velocity of granites with different grain sizes after thermal treatment: **a** and **b** For LF and HF waves, respectively

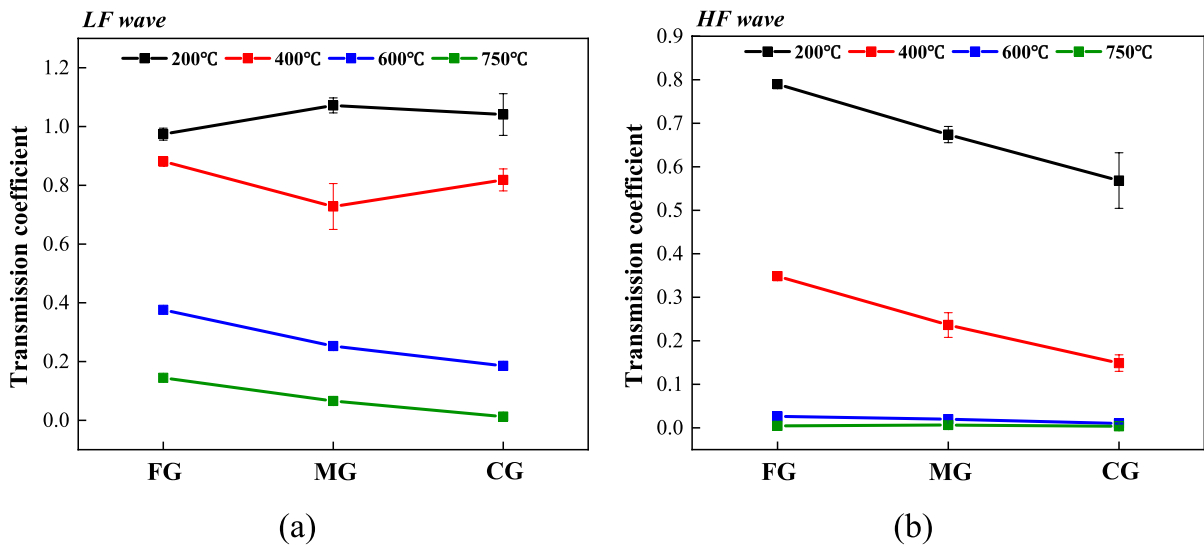


Fig. 8 Transmission coefficients of waves across granites with different grain sizes after thermal treatment: **a** LF wave; and **b** HF wave

3.2.2 Transmission coefficient

Figure 8a, b illustrate the transmission coefficients of LF and HF waves across thermally damaged granites with increasing grain size, respectively. The correlation between grain size and transmission coefficient was highly dependent on heating temperature and central frequency. When the temperature was 200 °C, the transmission coefficients of LF waves across granites varied with the grain size. The transmission coefficients of MG (1.07) and CG (1.04) granites were greater than 1, indicating that rock properties were reinforced due to the crack closure caused by crystal expansion at this temperature (i.e., thermal enhancing). In the contrast, the transmission coefficient of FG granite (0.97) was less than 1, which means that under the same condition, the occurrence of thermal cracking is more likely than that of crack closure (i.e., thermal degrading). This result indicated that the competitive relationship between thermal enhancing and degrading is influenced by grain size. With further increase in the temperature, the thermal rupture intensified and the transmission coefficients of rocks with different grain sizes were less than 1. As the temperature rose to 400 °C, the transmission coefficient was non-linearly related to the grain size. That is, the transmission coefficients of LF waves through MG granites were smaller than those through FG and

CG granites. This may be attributed to the aggravated structural fracture in the MG granite, as demonstrated in the SEM observation below. The transmission coefficient was negatively correlated with grain size beyond 600 °C. For the HF wave, variations in transmission coefficients are significantly different. The transmission coefficients of the HF waves through heat-treated granites were always less than 1 and tended to decrease with increasing grain size. The dependence of the transmission coefficient on grain size was more apparent at temperatures below 400 °C. It is noteworthy that, the transmission coefficient of the HF wave beyond 600 °C was quite small and fluctuated within a narrow range, thus the effect of grain size on the transmission coefficient could be ignored at high temperatures.

3.2.3 Peak PSD

Figure 9a, b present the evolution of peak PSD with increasing grain size for LF and HF ultrasonic waves across granites after different thermal treatments, respectively. The peak PSD of LF ultrasonic waves showed a subtle declining trend with increasing grain size. However, it is observed that the peak PSD of the LF wave through the MG granite at 400 °C is smaller than that through FG and CG granites, which

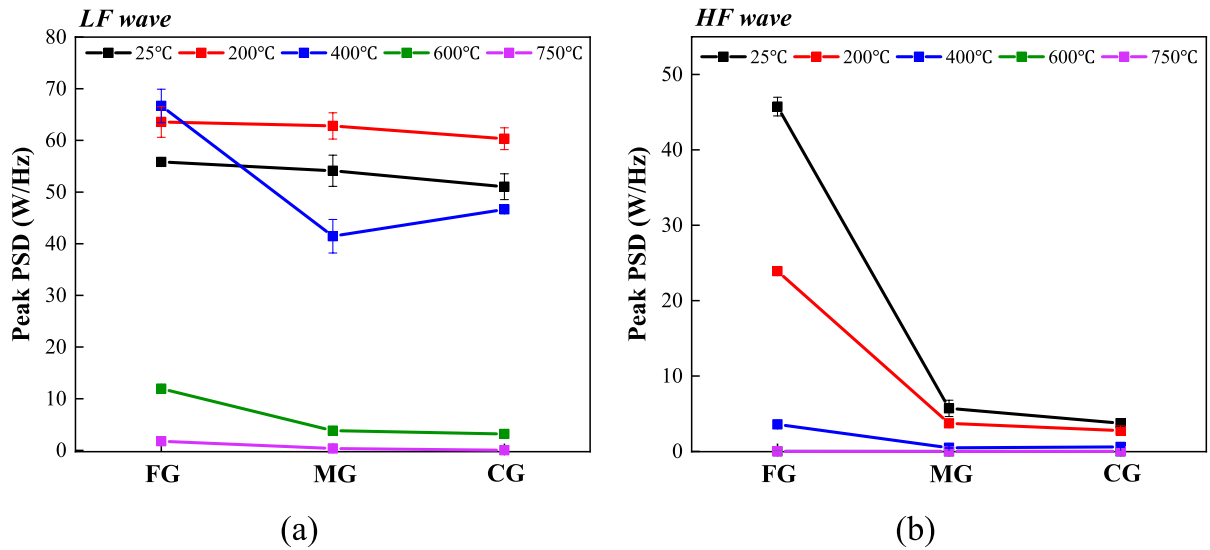


Fig. 9 Difference in the peak PSD of waves through granites with different grain sizes after heating: **a** and **b** for LF and HF waves, respectively. Note that the peak PSD across granite at 600 °C and 750 °C are similar and minor, without affecting the overall pattern

is similar to the transmission coefficient. In contrast, the peak PSD of HF ultrasonic waves decreased significantly with increasing grain size while the difference was more apparent at lower temperatures. For instance, at room temperature, the peak PSD of the

HF waves through FG granites was several times larger than those through MG and CG granites, which were 45.7, 5.7 and 3.7 W/Hz, respectively. In comparison, the peak PSDs of the HF waves through CG, FG and MG were 0.02, 0.01 and 0.006 W/Hz at the temperature of 600 °C, respectively.

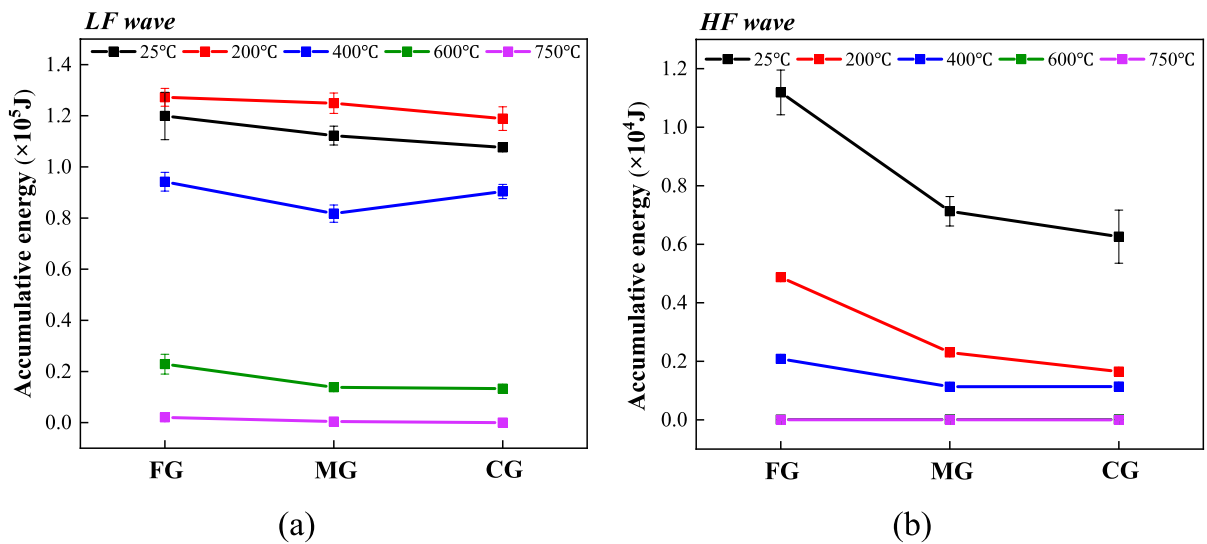


Fig. 10 The average accumulative energies of waves through granites with different grain sizes after heating: **a** LF waves; and **b** HF waves, respectively. Note that peak PSD and accu-

mulative energy of HF waves across granites at 600 °C and 750 °C is extremely small, which is not easy to indicate in the figure, but does not affect the overall trend

3.2.4 Accumulative energy

Figure 10a, b show the accumulative energy of LF and HF ultrasonic waves through granites after thermal treatment from 25 to 750 °C versus grain size, respectively. The accumulative energy of LF waves decreased steadily with increasing grain size, except for the specificity of the MG granite at 400 °C. For the HF wave, the drop in the accumulative energy with increasing grain size was greater, especially at temperatures below 400 °C. For instance, after heating at 200 °C, the accumulative energy of the HF wave across FG granites was 36% and 44% larger than those of MG and CG granites, respectively. In addition, it could be observed that the evolution of accumulative energy and peak PSD are similar, which indicates a uniform response of grain size to the frequency and energy characteristics of ultrasonic waves.

3.3 Microcrack evolution

Figure 11 shows the SEM images of CG granite specimens with increasing temperatures. When the heating temperature was 200 °C, it could be seen that crack extension and closure occur simultaneously. The intergranular micro-cracks initiated and expanded from the tip of primary defects, meanwhile, the pre-existing defects closed due to the crystal expansion. As the temperature increased to 400 °C, the generation and propagation of transgranular cracks implied an intensified destruction of the rock microstructure, accompanied by an attenuation of ultrasonic wave parameters. When the temperature reached 600 °C, transgranular cracks further developed and connected with intergranular cracks. The micro-crack network was formed basically, causing the crystal to break up and the particle size to dwindle, thereby aggravating the attenuation of ultrasonic wave properties. With the further increase in heating temperature (such as 750 °C), the network of cracks spread all over the rock. Compared with the observed images under 600 °C (Fig. 11c), only the width of cracks increased slightly. This phenomenon may be the reason for the small change in wave parameters after thermal treatment above 600 °C. Previous researches (Griffith et al. 2018; Zhai et al. 2022) showed the intergranular-transgranular-macroscopic crack transformation

pattern under the effect of thermal, which is consistent with the observations in this study.

As mentioned above, when the heating temperature is extremely high (e.g., 600 °C), the effect of grain size on crack evolution diminishes, owing to the cutting of crack networks (see Fig. 11c, d). Figure 12 shows SEM images of FG, MG and CG granites before and after heating at the temperature of 200 °C. When the grain size was relatively small (FG granite), i.e., 1.2 mm, minerals basically maintained their original crystalline forms, which could be explained that small crystals are more resilient to thermal stress (Ersoy et al. 2021). With an increase in grain size to 3.4 mm (MG granite), intergranular micro-cracks appeared to expand obviously, accompanied by the closure of intergranular cracks. As the grain size rose to 5 mm (CG granite), the extension length of intergranular micro-cracks in the specimens became larger, thereby reducing ultrasonic wave properties (as shown in Fig. 10). The experimental results on the greater development of intergranular cracks with increasing grain size are in agreement with previous researches (Shao et al. 2014; Nicco et al. 2020), reporting that narrow cracks develop into networks extensively in granites with a grain size of 1–7 mm, while that are few in granites with grain size less than 1 mm. The mechanism could be illustrated by Eberhardt et al. (1999), who found that longer grain boundaries and larger intergranular cracks could provide more continuous paths for growing cracks to propagate along.

The development of cracks in granites of FG and MG at 400 °C is demonstrated in Fig. 13a, b, respectively. It could be seen that transgranular cracks initiated and propagated steadily while the closure of primary cracks still occurred when the grain size was 1.2 mm (FG granite). As the grain size increased to 5 mm (CG granite), further development in the length of transgranular cracks could be observed (see Fig. 11b), leading to a decrease in wave properties. By comparison, an unusual observation in Fig. 13b is that transgranular cracks have been penetrated to separate the edge particle of mineral crystals when the grain size was 3.4 mm (MG granite), thus causing the relatively small wave parameters (Figs. 8a, 9a). This phenomenon is not found in samples with a grain size of 5 and 1.2 mm. It means that the matching of transgranular crack extension length and crystal size

Fig. 11 The SEM images of the CG granite before (left column) and after (right column) heating treatment at different temperatures: **a** 200 °C, **b** 400 °C, **c** 600 °C, **d** 750 °C

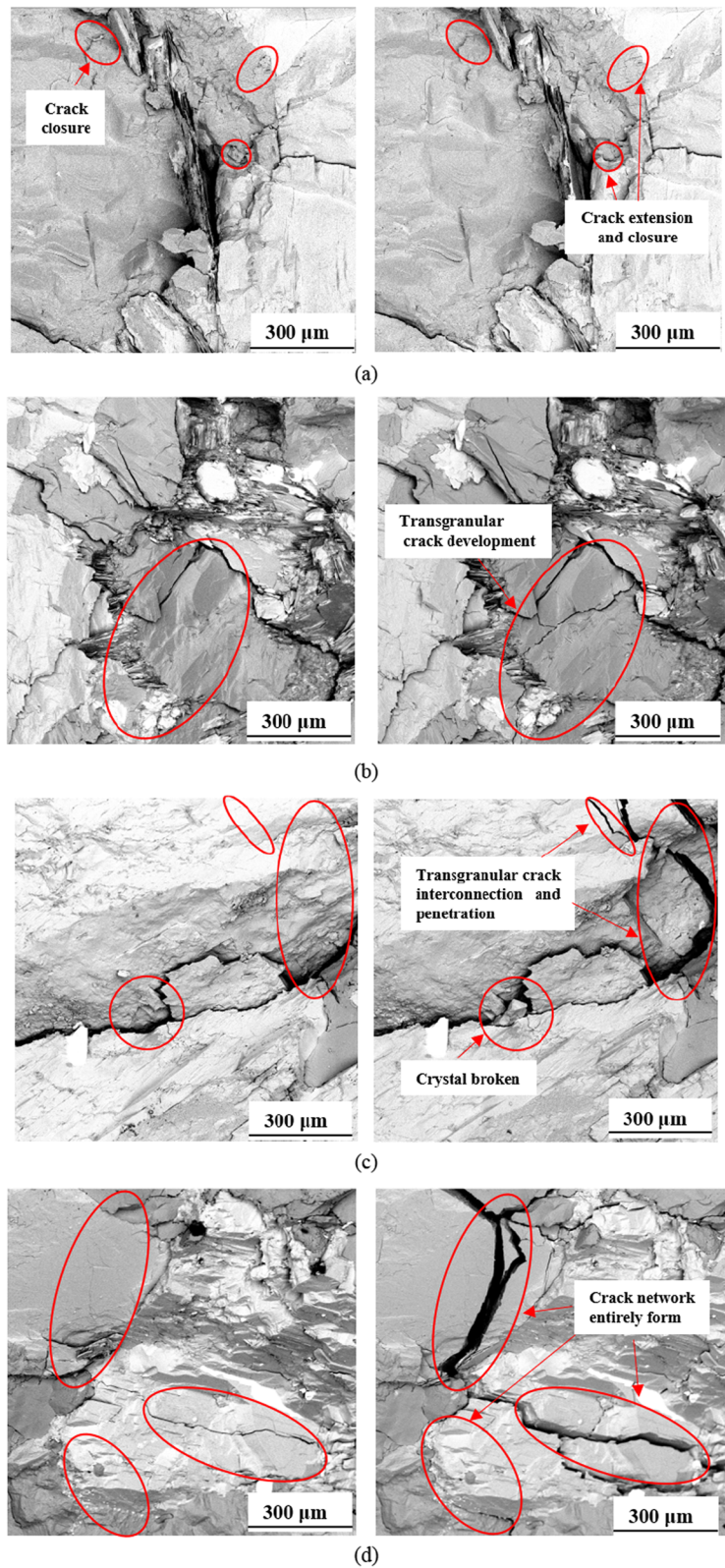


Fig. 12 The SEM images of granites with different grain sizes before (left column) and after (right column) heat treatment at 200 °C: **a** FG, **b** MG, **c** CG

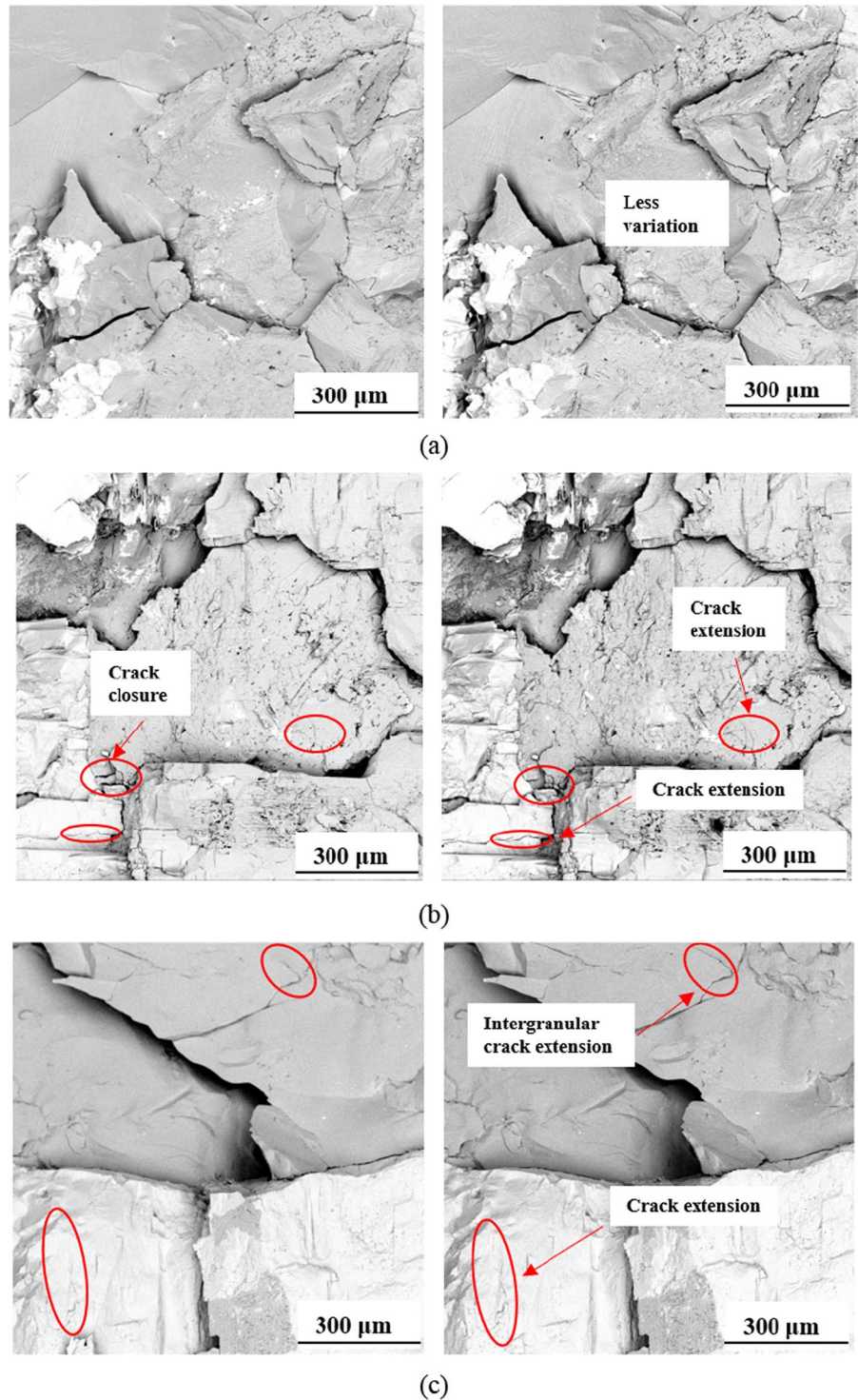
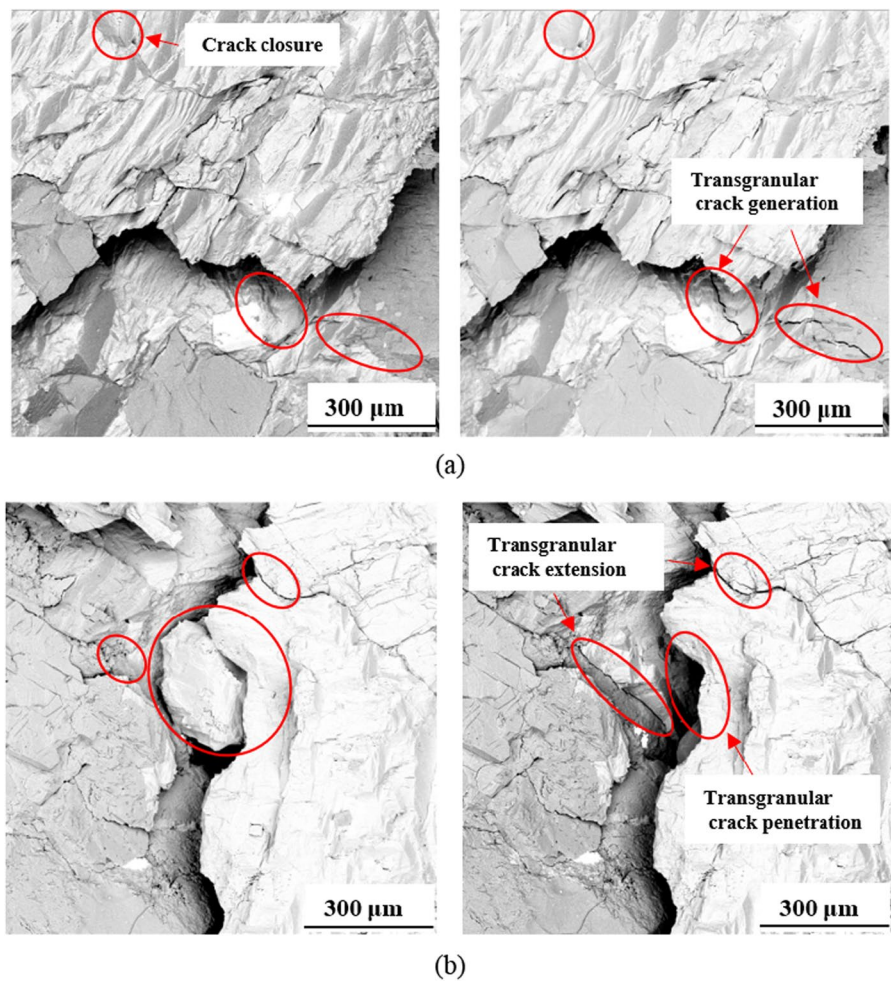


Fig. 13 The SEM images of granites with different grain sizes before (left column) and after (right column) heat treatment at 400 °C: **a** FG; and **b** MG



played a nonnegligible role in crack penetration. The conclusions of Sabri et al. (2016) and Feng et al. (2021) on the non-linear relation between rock properties and grain sizes (1–5 mm) also support the specificity of MG granite (3.4 mm) in this study.

4 Discussion

Findings in this paper reveal that the propagation behaviour of ultrasonic waves and the microcrack evolution in granites are highly dependent on the heating temperature and grain size. Specifically, the ultrasonic wave parameters across the granite decrease as the heating temperature and grain size increase, while the length and density of micro-cracks are larger. The existence of micro-cracks is generally considered to be the main reason for the attenuation of ultrasonic

waves (Jiang et al. 2018; Sun et al. 2022). This could be explained by the dispersion theory that the wave energy is converted into thermal energy and thus dissipated when the stress wave propagation through discontinuities, e.g., micro-cracks and micro-pores. In addition, the further growth of micro-cracks makes the rock more fragmented and the stress waves more significantly dispersed, leading to more energy dissipation and amplitude attenuation.

Apart from heating temperature and grain size, the seismic responses of granites are affected by the central frequency of the incident waves. It could be seen that the characteristics of LF and HF waves across the same specimen after heat treatment tests are various, i.e., possible with or without thermal enhancement. There may be a competitive mechanism between crack closure and extension in response to thermal action, and the enhancement or degradation of rock

properties depends on the outcome of this competition (Zhao et al. 2018; Zhai et al. 2022). For instance, the properties of LF waves increase from 25 to 200 °C (see Fig. 4a), which could be attributed to the dominant role of crack closure. By comparison, it is noticeable that there is a continuous attenuation trend of the HF wave (as shown in Fig. 4b), which implies that crack extension may be dominant. In fact, similar results can be found from previous researches on the physical and mechanical parameters of rocks, e.g., P- and S-wave velocity (Jiang et al. 2018; Kumari et al. 2019; Ersoy et al. 2021). It is hard to explain the difference between rock properties, but the results in this paper are related to the frequency of incident waves, which is known that the HF wave propagation is mainly influenced by the development of micro-cracks rather than crack closure (as shown in Fig. 6). To sum up, it is advisable to describe thermal enhancing in terms of specific parameters and determine whether crack closure or extension dominates combining more macroscopic and microscopic parameters.

The above SEM results interpret the microscopic mechanism of the crack evolution under the combined effect of heating temperature and grain size. On this basis, the experimental results of ultrasonic attenuation in Sect. 3 could be well understood. To quantify the deterioration degree of rock microstructures caused by the crack evolution of granites with different grain sizes after heating, we define the damage factor by the change of microcrack area. The SEM images are binarized with ImageJ software to highlight the changes in micro-cracks. The threshold segmentation of greyscale images is determined

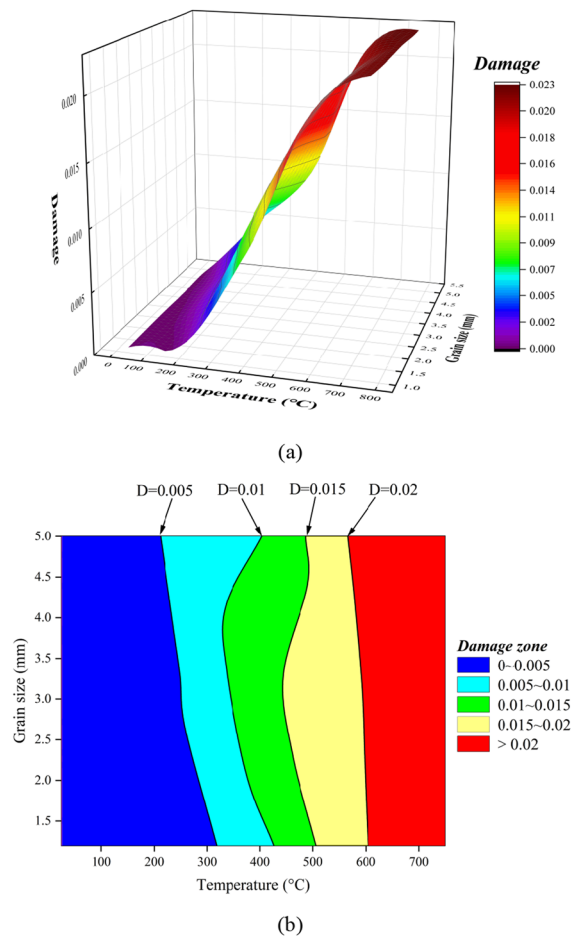


Fig. 15 The damage factors of granites: **a** Versus temperature and grain size; and **b** projection interval in the temperature-grain size plane

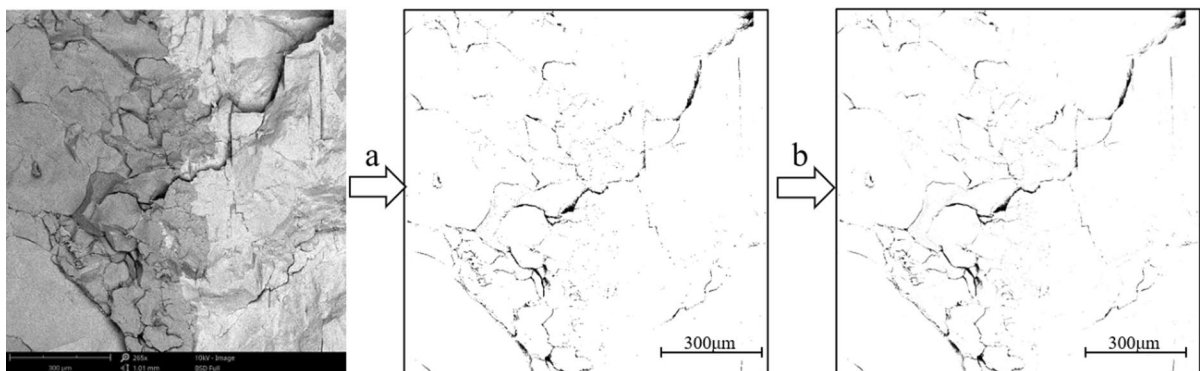


Fig. 14 The thresholding process of SEM images: **a** Binarization; and **b** denoising and smoothing

by the minimum cross-entropy threshold iteration method, followed by a final denoising and smoothing of the images. The whole processing of SEM images is illustrated in Fig. 14. And the damage factor D is calculated as:

$$D = 1 - \frac{S_{tot} - S_h}{S_{tot} - S_0} \quad (7)$$

where S_{tot} is the total area of the processed images, S_0 and S_h are the area of black pixels (microdefects) in the processed images before and after heating treatment, respectively. The presented values of the damage factor for each sample are the average of three processed images.

The damage factor defined by the variation of micro-cracks in the binarized image can strongly reflect the combined effects of heating temperature and grain size on the attenuation of wave properties. Figure 15a represents the damage factors of granites versus temperature and grain size. It could be concluded that the damage factor rises moderately with increasing temperature and grain size, corresponding to a continuous decreasing trend of wave characteristic parameters (see Sect. 3). The damage zone could be equally classified into five degrees, as shown in Fig. 15b. When the damage factor is relatively low (e.g., $D=0.005$), the grain size is negatively linearly related to temperature in determining damage. As the damage factor increases ($0.01 < D < 0.015$), the damage isoline is bending, especially in the medium grain size range. At this damage phase, granites with medium grain sizes (around 3 mm) have greater damage values for the same temperature conditions, which is consistent with the smaller wave parameters of MG granite at 400 °C in previous ultrasonic tests (see Figs. 8, 9). When the damage factor is high ($D=0.02$), the damage isoline converges to a straight line perpendicular to the temperature, indicating that the damage factor is mainly controlled by heating temperature and the effect of grain size is limited. Note that the damage factor determined by the change of micro-cracks in this study is relatively small compared to those defined by macroscopic parameters such as wave velocity, AE counts, elastic modulus, strength and permeability (Chaki et al. 2008; Zhu et al. 2017, 2020; Gautam et al. 2018; Zhang et al. 2021a, b; Hu et al. 2022). This could be explained by the fact that the increment of microdefects area

consistently occupies only a minor proportion of the specimen section, while it can cause a rapid destabilization of the rock. Similar findings were observed for the damage factor defined by the void space area in the sliced CT image (Yang and Liu 2007; Ma et al. 2016). Moreover, the selection of the observation scale also needs to be taken into account when determining the percentage of microcrack area, although it may influence the accuracy rather than the overall trend (Qin and Xu 2016). It is preferable to consider the influence of the observation scale in exploring the accurate characterization of damage factors by microscopic parameters in the future.

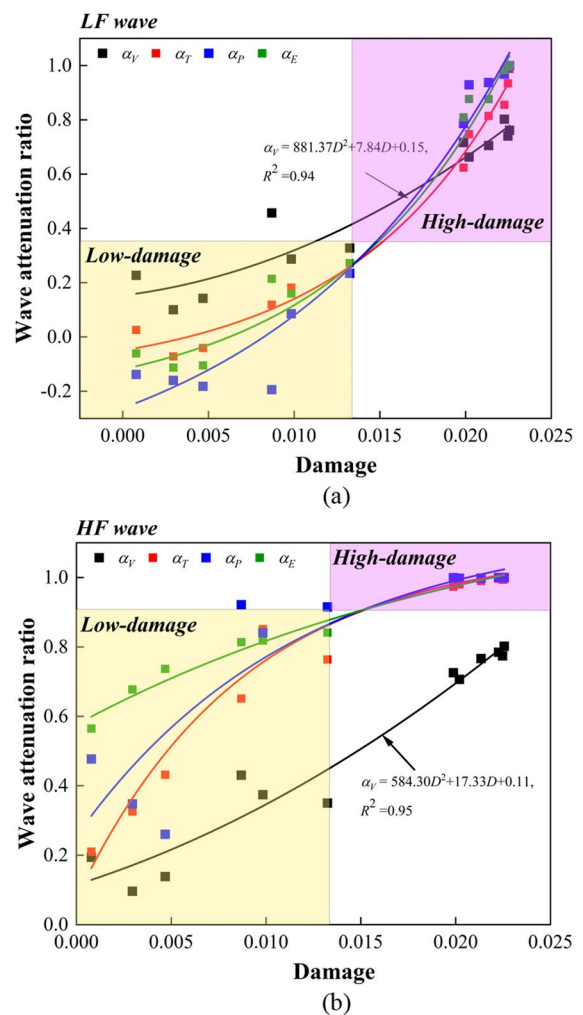


Fig. 16 The relationship between ultrasonic wave attenuation ratios and damage factors: **a** and **b** For the LF and HF ultrasonic wave, respectively

The results of ultrasonic transmission experiments showed that the evolution of various characteristic parameters of ultrasonic wave signals is different under a given grain size and heat treatment temperature. Besides, the influence of the central frequency on wave attenuation is also significant. These results implied that there are differences in the sensitivity of ultrasonic wave characteristic parameters with various central frequencies to the damage degree under the combined influence of heating temperature and grain size. In order to pick out a suitable evaluation indicator for optimizing the accuracy of non-destructive testing in rock stability assessment, the attenuation ratio of wave parameters as a function of damage degree is shown in Fig. 16, where the attenuation ratios of wave parameters α_i are defined as:

$$\alpha_i = \frac{WP_{0,i} - WP_{h,i}}{WP_{0,i}} \tag{8}$$

where $WP_{0,i}$ and $WP_{h,i}$ are the measured values of wave characteristics parameters across granites at room temperature and high temperature, respectively, i includes V , T , P , and E (i.e., the wave velocity, transmission coefficient, peak PSD and accumulative energy, respectively). Regardless of the central frequency, the attenuation ratio of the wave velocity is quadratically related to the damage factor. For the other three characteristic parameters, after many attempts, an exponential function could give the best approximation (as shown in Fig. 16), which is in a form of

$$\alpha_i = a \times \exp(b \times D) - c \tag{9}$$

where constant a , b , c and the correlation coefficients R^2 for three types of wave properties are determined after the best fitting and are listed in Table 2. For the LF wave, the up-concave fitting curves (a and $b > 0$) indicated that the increasing rate of the attenuation

ratio grows with increasing damage. It could be concluded from Fig. 16a that the peak PSD maintains the largest change magnitude among the three wave characteristic parameters for the same damage increment condition. For the HF wave, the attenuation ratio increases at a gradually decreasing rate as the damage factor increases (a and $b < 0$), with the greatest variation rate of transmission coefficient.

Notably, our SEM observations (see Fig. 13) suggested that the penetration of transgranular cracks initially occurs in the MG granite (3.4 mm) at 400 °C (damage value of 0.013 in Fig. 15), indicating severe destruction of the internal structure and a reduction in the bearing capacity of the rock (Zhang et al. 2018). It could be seen from Fig. 16 that when the damage factor is greater than 0.013, the wave attenuation ratios of LF waves increase sharply, and those of HF waves tend to 1 (complete attenuation), reflecting the intensified deterioration of rock properties. Similar findings were observed for the physical and mechanical properties of rocks after the temperature threshold (Yin et al. 2021; Feng et al. 2021). Therefore, based on the deterioration degree of the rock structure, the response of wave attenuation ratio to damage could be simply divided into two stages, i.e., low- (below 0.013) and high- (over 0.013) damage stages, as shown in Fig. 16. At different damage stage, distinct evaluation indicators should be applied to meet the research purpose and accuracy requirements (Jin et al. 2019; Hu et al. 2022). During the high-damage stage, the rock is gradually destabilized and the internal structure is locally broken, hence it is desired to characterize the damage degree precisely by wave parameters with high sensitivity to ensure the safety of the rock. After comparison, the peak PSD of the LF wave has the highest sensitivity to damage among all characteristic parameters. At the low-damage stage, we pay more attention to thermal rupture from a conservative estimate of engineering stability. It can be

Table 2 Constants and correlation coefficients for different ultrasonic wave parameters after best fitting

Fitting equation $a \times \exp(b \times D) - c$	LF wave			HF wave		
	α_T	α_P	α_E	α_T	α_P	α_E
a	0.10	0.33	0.14	-1.01	-0.90	-0.70
b	105.26	71.43	98.04	-113.64	-85.25	-40.0
c	-0.15	-0.59	-0.26	1.09	1.15	1.28
R^2	0.99	0.98	0.98	0.97	0.80	0.97

seen that the transmission coefficient of the HF wave attenuates continuously in the low-damage region and is much more sensitive than the other three wave parameters. Above all, according to the sensitivity of propagation features, the peak PSD of the LF wave and the transmission coefficient of the HF wave are eventually selected as the optimal stress wave indicators for evaluating the damage state of granites at high- and low-damage stages, respectively.

Many deep geotechnical engineering activities are carried out under high temperatures and complex geological conditions. The findings in this paper could provide guidance for site selection and stability assessment in geothermal engineering applications. The selection of rocks with reasonable grain sizes has a significant impact on improving geothermal engineering productivity. For example, CG and FG granites may be more favourable choices for geothermal energy development objects than MG granites (as shown in Fig. 13), since the maximum temperature of the surrounding rock may reach approximately 400 °C due to the geological occurrence conditions (Hu et al. 2019). In addition, the transmission coefficient of LF waves can serve high-temperature projects such as underground coal gasification mining at temperatures beyond 600 °C (Xiang et al. 2018), while the transmission coefficient of HF waves is more suitable for low-temperature (less than 200 °C) projects such as nuclear waste storage (Li et al. 2011), as illustrated in Fig. 16.

5 Conclusions

The main conclusions of this paper are summarized as follows:

- (1) Heating temperature and grain size have a remarkable impact on wave propagation across the granites. With increasing temperature, the wave velocity, transmitted coefficient, peak PSD and accumulative energy generally decrease, and the dominant frequency and energy concentration area shift from the higher to lower frequency region. The wave velocity decreases first and then increases with increasing grain size, while the transmitted coefficient, peak PSD and accumula-

tive energy are linearly negatively correlated with grain size. The effect of grain size on wave propagation is more pronounced at low temperatures.

- (2) The seismic responses of heated granites are affected by the bandwidth (central frequency) of the incident waves. The wave attenuation of high-frequency waves is stronger than that of low-frequency waves. The propagation features of low-frequency waves, especially the peak PSD, could present a slight increase with increasing temperature in the low temperature range (from 25 to 200 °C). There is no such phenomenon for the high-frequency wave.
- (3) The crack evolution is significantly influenced by the combination of grain size and heating temperature, which determines the wave propagation behaviour of granites. At low temperatures, the effect of grain size on the development of intergranular or transgranular cracks should be considered. While at high temperatures, thermal cracks extend in the form of networks regardless of grain size.
- (4) A damage factor defined by the change of micro-crack area is proposed and adopted to consider the combined effect of heating temperature and grain size on wave propagation. The peak PSD of the low-frequency wave and the transmission coefficient of the high-frequency wave are appropriate as the optimal wave indicators for evaluating the deterioration of granites at high- and low-damage stages, respectively.

Acknowledgements This research was financially supported by National Key R&D Program of China (No. 2022YFC3004602), Program for Guangdong Introducing Innovative and Entrepreneurial Teams (No. 2019ZT08G315) and Shenzhen Fundamental Research Program (No. JCYJ20220818095605012; No. JCYJ20210324093402006).

Author contribution EZ: Methodology, Formal analysis, Investigation, Writing—original draft. TZ: Methodology, Writing—review and editing. JZ: Conceptualization, Methodology, Writing—review and editing, Supervision, Funding acquisition.

Availability of data and materials All participants state that the contents of the article do not contain unknown, fake or false data. The data generated in the present study are available from the corresponding author upon reasonable request.

Declarations

Ethics approval and consent to participate Not applicable.

Consent for publication The authors confirm that we understand Geomechanics and Geophysics for Geo-Energy and Geo-Resources is an open access journal that levies an article processing charge per articles accepted for publication. By submitting my article, I agree to pay this charge in full if my article is accepted for publication. We have read the Springer journal policies on author responsibilities and submit this manuscript in accordance with those policies. Springer Nature or its licensor holds exclusive rights to this article under a publishing agreement with the author(s) or other rightsholder(s); author self-archiving of the accepted manuscript version of this article is solely governed by the terms of such publishing agreement and applicable law.

Competing interests The authors declare no competing interests.

Open Access This article is licensed under a Creative Commons Attribution 4.0 International License, which permits use, sharing, adaptation, distribution and reproduction in any medium or format, as long as you give appropriate credit to the original author(s) and the source, provide a link to the Creative Commons licence, and indicate if changes were made. The images or other third party material in this article are included in the article's Creative Commons licence, unless indicated otherwise in a credit line to the material. If material is not included in the article's Creative Commons licence and your intended use is not permitted by statutory regulation or exceeds the permitted use, you will need to obtain permission directly from the copyright holder. To view a copy of this licence, visit <http://creativecommons.org/licenses/by/4.0/>.

References

- ASTM Standard D2845-08 (2008) standard test method for laboratory determination of pulse velocities and ultrasonic elastic constants of rock. ASTM International, West Conshohocken
- Benavente D, Galiana-Merino JJ, Pla C, Martinez-Martinez J, Crespo-Jimenez D (2020) Automatic detection and characterisation of the first P- and S-wave pulse in rocks using ultrasonic transmission method. *Eng Geol* 266:105474. <https://doi.org/10.1016/j.enggeo.2020.105474>
- Cerrillo C, Jiménez A, Rufo M, Paniagua J, Pachón FT (2014) New contributions to granite characterization by ultrasonic testing. *Ultrasonics* 54(1):156–167. <https://doi.org/10.1016/j.ultras.2013.06.006>
- Chaki S, Takarli M, Agbodjan WP (2008) Influence of thermal damage on physical properties of a granite rock: porosity, permeability and ultrasonic wave evolutions. *Constr Build Mater* 22(7):1456–1461. <https://doi.org/10.1016/j.conbuildmat.2007.04.002>
- Chen J, Yin TY, Kim JY, Xu Z, Yao YP (2017) Characterization of thermal damage in sandstone using the second harmonic generation of standing waves. *Int J Rock Mech Min Sci* 91:81–89. <https://doi.org/10.1016/j.ijrmms.2016.11.014>
- Dehghani B, Amirkiyai V, Ebrahimi R, Ahmadi H, Mohammadzamani D, Zavareh SB (2020) Thermal loading effect on P-wave form and power spectral density in crystalline and non-crystalline rocks. *Arab J Geosci* 13(16):779–787. <https://doi.org/10.1007/s12517-020-05779-9>
- Ding PB, Wang D, Li XY (2020) An experimental study on scale-dependent velocity and anisotropy in fractured media based on artificial rocks with controlled fracture geometries. *Rock Mech Rock Eng* 53(7):3149–3159. <https://doi.org/10.1007/s00603-020-02095-2>
- Dwivedi RD, Goel RK, Prasad VVR, Sinha A (2008) Thermo-mechanical properties of Indian and other granites. *Int J Rock Mech Min Sci* 45(3):303–315. <https://doi.org/10.1016/j.ijrmms.2007.05.008>
- Eberhardt E, Stimpson B, Stead D (1999) Effects of grain size on the initiation and propagation thresholds of stress-induced brittle fractures. *Rock Mech Rock Eng* 32(2):81–99. <https://doi.org/10.1007/s006030050026>
- Ersoy H, Atalar C, Sunnetci MO, Kolaylı H, Karahan M, Ersoy AF (2021) Assessment of damage on geo-mechanical and micro-structural properties of weak calcareous rocks exposed to fires using thermal treatment coefficient. *Eng Geol* 284:106046. <https://doi.org/10.1016/j.enggeo.2021.106046>
- Fan LF, Wu ZJ, Wan Z, Cao JW (2017) Experimental investigation of thermal effects on dynamic behavior of granite. *Appl Therm Eng* 125:94–103. <https://doi.org/10.1016/j.applthermaleng.2017.07.007>
- Feng ZJ, Zhao YS, Liu DN (2021) Permeability evolution of thermally cracked granite with different grain sizes. *Rock Mech Rock Eng* 54(4):1953–1967. <https://doi.org/10.1007/s00603-020-02361-3>
- Fjær E, Stroisz AM, Holt RM (2013) Elastic dispersion derived from a combination of static and dynamic measurements. *Rock Mech Rock Eng* 46(3):611–618. <https://doi.org/10.1007/s00603-013-0385-8>
- Galiana-Merino JJ, Rosa-Herranz JL, Rosa-Cintas S, Martinez-Esplá JJ (2013) SeismicWaveTool: continuous and discrete wavelet analysis and filtering for multichannel seismic data. *Comput Phys Commun* 184(1):162–171. <https://doi.org/10.1016/j.cpc.2012.08.008>
- Gautam PK, Verma AK, Sharma P, Singh TN (2018) Evolution of thermal damage threshold of Jalore granite. *Rock Mech Rock Eng* 51(9):2949–2956. <https://doi.org/10.1007/s00603-018-1493-2>
- Griffiths L, Lengline O, Heap MJ, Baud P, Schmittbuhl J (2018) Thermal cracking in Westerly granite monitored using direct wave velocity, coda wave interferometry, and acoustic emissions. *J Geophys Res-Solid Earth* 123(3):2246–2261. <https://doi.org/10.1002/2017jb015191>
- Hu XD, Song XZ, Liu Y, Cheng Z, Ji JY, Shen ZH (2019) Experiment investigation of granite damage under the high-temperature and high-pressure supercritical water

- condition. *J Pet Sci Eng* 180:289–297. <https://doi.org/10.1016/j.petrol.2019.05.031>
- Hu YF, Hu YQ, Zhao GK, Jin PH, Zhao ZR, Li C (2022) Experimental investigation of the relationships among P-wave velocity, tensile strength, and mode-I fracture toughness of granite after high-temperature treatment. *Nat Resour Res* 31(2):801–816. <https://doi.org/10.1007/s11053-022-10020-3>
- Insera C, Biwa S, Chen YQ (2013) Influence of thermal damage on linear and nonlinear acoustic properties of granite. *Int J Rock Mech Min Sci* 62:96–104. <https://doi.org/10.1016/j.ijrmms.2013.05.001>
- Jiang GH, Zuo JP, Li LY, Ma T, Wei X (2018) The evolution of cracks in Maluanshan granite subjected to different temperature processing. *Rock Mech Rock Eng* 51(6):1683–1695. <https://doi.org/10.1007/s00603-018-1403-7>
- Jin PH, Hu YQ, Shao JX, Zhao GK, Zhu XZ, Li C (2019) Influence of different thermal cycling treatments on the physical, mechanical and transport properties of granite. *Geothermics* 78:118–128. <https://doi.org/10.1016/j.geothermics.2018.12.008>
- Kumari WGP, Beaumont DM, Ranjith PG, Perera MSA, Avanthi Isaka BL, Khandelwal M (2019) An experimental study on tensile characteristics of granite rocks exposed to different high-temperature treatments. *Geomech Geophys Geo-Energy Geo-Resour* 5(1):47–64. <https://doi.org/10.1007/s40948-018-0098-2>
- Li J, Yim MS, Mcnelis D (2011) A simplified methodology for nuclear waste repository thermal analysis. *Ann Nucl Energy* 38(2–3):243–253. <https://doi.org/10.1016/j.anucene.2010.11.002>
- Li ZH, Wong LNY, Teh CI (2020) Influence of thermal and mechanical loading on development of microcracks in granite. *Rock Mech Rock Eng* 53(5):2035–2051. <https://doi.org/10.1007/s00603-019-02030-0>
- Liang ZZ, Xue RX, Xu NW, Li WR (2020) Characterizing rockbursts and analysis on frequency-spectrum evolutionary law of rockburst precursor based on microseismic monitoring. *Tunn Undergr Space Technol* 105:103564. <https://doi.org/10.1016/j.tust.2020.103564>
- Ma TS, Yang CH, Chen P, Wang XD, Guo YT (2016) On the damage constitutive model for hydrated shale using CT scanning technology. *J Nat Gas Sci Eng* 28:204–214. <https://doi.org/10.1016/j.jngse.2015.11.025>
- Machek M, Spacek P, Ulrich S, Heidelbach F (2007) Origin and orientation of microporosity in eclogites of different microstructure studied by ultrasound and microfabric analysis. *Eng Geol* 89(3–4):266–277. <https://doi.org/10.1016/j.enggeo.2006.11.001>
- Menendez B, David C, Darot M (1999) A study of the crack network in thermally and mechanically cracked granite samples using confocal scanning laser microscopy. *Phys Chem Earth (a)* 24(7):627–632. [https://doi.org/10.1016/S1464-1895\(99\)00091-5](https://doi.org/10.1016/S1464-1895(99)00091-5)
- Nicco M, Holley EA, Hartlieb P, Pfaff K (2020) Textural and mineralogical controls on microwave-induced cracking in granites. *Rock Mech Rock Eng* 53(10):4745–4765. <https://doi.org/10.1007/s00603-020-02189-x>
- Qin X, Xu QJ (2016) Statistical analysis of initial defects between concrete layers of dam using X-ray computed tomography. *Constr Build Mater* 125:1101–1113. <https://doi.org/10.1016/j.conbuildmat.2016.08.149>
- Qiu J (1991) Brief introduction of a classification of volcanic rocks recommendations of the IUGS subcommission on the systematics of igneous rocks. *Geoscience* 5(4):457–468 (in Chinese)
- Sabri M, Ghazvinian A, Nejati HR (2016) Effect of particle size heterogeneity on fracture toughness and failure mechanism of rocks. *Int J Rock Mech Min Sci* 81:79–85. <https://doi.org/10.1016/j.ijrmms.2015.11.002>
- Sajid M, Coggan J, Arif M, Andersen J, Rollinson G (2016) Petrographic features as an effective indicator for the variation in strength of granites. *Eng Geol* 202:44–54. <https://doi.org/10.1016/j.enggeo.2016.01.001>
- Sang GJ, Liu SM, Elsworth D (2020) Quantifying fatigue-damage and failure-precursors using ultrasonic coda wave interferometry. *Int J Rock Mech Min Sci* 131:104366. <https://doi.org/10.1016/j.ijrmms.2020.104366>
- Shao SS, Wasantha PLP, Ranjith PG, Chen BK (2014) Effect of cooling rate on the mechanical behavior of heated Strathbogie granite with different grain sizes. *Int J Rock Mech Min Sci* 70:381–387. <https://doi.org/10.1016/j.ijrmms.2014.04.003>
- Shao SS, Ranjith PG, Wasantha PLP, Chen BK (2015) Experimental and numerical studies on the mechanical behaviour of Australian Strathbogie granite at high temperatures: an application to geothermal energy. *Geothermics* 54:96–108. <https://doi.org/10.1016/j.geothermics.2014.11.005>
- Sun Y, Zhai C, Xu JZ, Yu X, Cong YZ, Zheng YF, Tang W, Li YJ (2022) Damage and failure of hot dry rock under cyclic liquid nitrogen cold shock treatment: a non-destructive ultrasonic test method. *Nat Resour Res* 31(1):261–279. <https://doi.org/10.1007/s11053-021-10005-8>
- Tian WL, Yang SQ, Huang YH, Hu B (2020) Mechanical behavior of granite with different grain sizes after high-temperature treatment by particle flow simulation. *Rock Mech Rock Eng* 53(4):1791–1807. <https://doi.org/10.1007/s00603-019-02005-1>
- Vajdova V, Prikryl R, Pros Z, Klima K (1999) The effect of rock fabric on P-wave velocity distribution in amphibolites. *Phys Earth Planet Inter* 114:39–47. [https://doi.org/10.1016/S0031-9201\(99\)00044-8](https://doi.org/10.1016/S0031-9201(99)00044-8)
- Wang CS, Wang LQ, Karakus M (2019) A new spectral analysis method for determining the joint roughness coefficient of rock joints. *Int J Rock Mech Min Sci* 113:72–82. <https://doi.org/10.1016/j.ijrmms.2018.11.009>
- Xiang XN, Gong GC, Shi Y, Cai YC, Wang CH (2018) Thermodynamic modeling and analysis of a serial composite process for biomass and coal co-gasification. *Renew Sustain Energy Rev* 82:2768–2778. <https://doi.org/10.1016/j.rser.2017.10.008>
- Yang GS, Liu H (2007) Study on the rock damage characteristics based on the technique of CT image processing. *J China Coal Soc* 32(5):463–468. <https://doi.org/10.3321/j.issn:0253-9993.2007.05.004>
- Yang SQ, Ranjith PG, Jing HW, Tian WL, Ju Y (2017) An experimental investigation on thermal damage and failure mechanical behavior of granite after exposure to different high temperature treatments. *Geothermics* 65:180–197. <https://doi.org/10.1016/j.geothermics.2016.09.008>

- Yang H, Duan HF, Zhu JB (2019) Ultrasonic P-wave propagation through water-filled rock joint: an experimental investigation. *J Appl Geophys* 169:1–14. <https://doi.org/10.1016/j.jappgeo.2019.06.014>
- Yang H, Duan HF, Zhu JB (2020) Effects of filling fluid type and composition and joint orientation on acoustic wave propagation across individual fluid-filled rock joints. *Int J Rock Mech Min Sci* 128:104248. <https://doi.org/10.1016/j.ijrmms.2020.104248>
- Yin WT, Feng ZJ, Zhao YS (2021) Effect of grain size on the mechanical behaviour of granite under high temperature and triaxial stresses. *Rock Mech Rock Eng* 54(2):745–758. <https://doi.org/10.1007/s00603-020-02303-z>
- Zhai TQ, Zhu JB, Zhou CT, Yang T (2022) Experimental investigation of the effect of thermal treatment on shear characteristics of healed rock joints. *Int J Rock Mech Min Sci* 152:105074. <https://doi.org/10.1016/j.ijrmms.2022.105074>
- Zhang WQ, Sun Q, Zhang YL, Wang B, Xue L, Kong FF (2018) Porosity and wave velocity evolution of granite after high-temperature treatment: a review. *Environ Earth Sci* 77(9):350–362. <https://doi.org/10.1007/s12665-018-7514-3>
- Zhang ZB, Wang EY, Zhang YH, Yang S, Liu XN, Ali M, Qi G (2019) Analysis on the time-frequency characteristics of ultrasonic waveform of coal under uniaxial loading. *Fractals* 27(6):1950100. <https://doi.org/10.1142/S0218348X19501007>
- Zhang B, Tian H, Dou B, Zheng J, Chen J, Zhu ZN, Liu HW (2021a) Macroscopic and microscopic experimental research on granite properties after high-temperature and water-cooling cycles. *Geothermics* 93:102079. <https://doi.org/10.1016/j.geothermics.2021.102079>
- Zhang YL, Zhao GF, Wei XD, Li HB (2021b) A multifrequency ultrasonic approach to extracting static modulus and damage characteristics of rock. *Int J Rock Mech Min Sci* 148:104925. <https://doi.org/10.1016/j.ijrmms.2021.104925>
- Zhao ZH, Liu ZN, Pu H, Li X (2018) Effect of thermal treatment on Brazilian tensile strength of granites with different grain size distributions. *Rock Mech Rock Eng* 51(4):1293–1303. <https://doi.org/10.1007/s00603-018-1404-6>
- Zhou HW, Xie H (2004) Anisotropic characterization of rock fracture surfaces subjected to profile analysis. *Phys Lett A* 325(5–6):355–362. <https://doi.org/10.1016/j.physleta.2004.04.006>
- Zhu SY, Zhang WQ, Sun Q, Deng S, Geng JS, Li CM (2017) Thermally induced variation of primary wave velocity in granite from Yantai: experimental and modeling results. *Int J Therm Sci* 114:320–326. <https://doi.org/10.1016/j.ijthermalsci.2017.01.008>
- Zhu JB, Zhai TQ, Liao ZY, Yang SQ, Liu XL, Zhou T (2020) Low-amplitude wave propagation and attenuation through damaged rock and a classification scheme for rock fracturing degree. *Rock Mech Rock Eng* 53(9):3983–4000. <https://doi.org/10.1007/s00603-020-02162-8>

Publisher's Note Springer Nature remains neutral with regard to jurisdictional claims in published maps and institutional affiliations.